Multirotor Systems Using Three Shrouded Wind Turbines for Power Output Increase

Watanabe, Koichi
Renewable Energy Utilization Research Unit, Kyushu University Platform of Inter/Transdisciplinary Energy Research

Ohya, Yuji
Winder Engineering Division, Research Institute for Applied Mechanics, Kyushu University

出版情報：Journal of Energy Resources Technology. 141 (5), pp.051211-1-051211-8, 2019-04-04. American Society of Mechanical Engineers
バージョン：

Koichi Watanabe
Renewable Energy Utilization Research Unit,
Kyushu University Platform of
Inter/Transdisciplinary Energy Research,
6-1 Kasuga-Koen,
Kasuga 816-8580, Japan
e-mail: koichi-watanabe@riam.kyushu-u.ac.jp

Yuji Ohya
Professor
Winder Engineering Division,
Research Institute for Applied Mechanics,
Kyushu University,
6-1 Kasuga-Koen,
Kasuga 816-8580, Japan
e-mail: ohya@riam.kyushu-u.ac.jp

Multirotor Systems Using Three Shrouded Wind Turbines for Power Output Increase

Brimmed-diffuser augmented wind turbines (B-DAWTs) can significantly increase the performance of the rotor. Multirotor systems (MRSs) have a lot of merits such as significant saving mass and overall cost of the wind turbine system. In the present research, B-DAWTs are studied in a MRS. In wind tunnel experiments, the power output and aerodynamics of three B-DAWTs placed in close vicinity have been investigated. The results show a significant increase of up to 12% in total power output of the MRS with B-DAWTs compared to the sum of the stand-alone (SA) same turbines. The accelerated gap flows between B-DAWTs in a MRS cause lowered pressure regions due to vortex interaction behind the brimmed diffusers and draw more wind into turbines.
[DOI: 10.1115/1.4042971]

1 Introduction

Wind power energy has been attracting attention as having some great potential of green energy. In order to increase the output from such a wind turbine so as to generate a sufficient amount of electric power, supersized (very large scale) wind turbines have become the global mainstream. Specifically, development has been performed for such wind turbines having a diameter of 100 m or more so as to output electric power on the order of several megawatts. Thus, the wind turbine industry has seen innovations leading to growing size of turbines of currently over 140 m in diameter. However, as the scale of the wind turbine becomes greater, the cost gets higher, and the failure rate becomes larger [1,2]. In addition, those supersized wind turbines lead to social problems such as increased noise (aerodynamic noise) that occurs due to the wind turbines, increased risk of bird strike, degradation of the surrounding landscape due to such large-scale wind turbines or sharp blades, and so on. Accordingly, it is difficult for local people to accept such supersized wind turbines, and that leads difficulties in installing such wind turbines. That is a big issue.

As pointed out by some recent studies, scaling of blades has its limitations. Therefore, advantages of multirotor systems (MRSs) concepts have been suggested by Jamison and Branney [3]. This system consists of many small or medium size wind turbines in the same vertical plane with small gaps supported by one tower [4]. According to Jamieson [5], instead of a large single wind turbine, by using a system of n smaller wind turbines, the power output does not change but the weight ratio becomes $1/\sqrt{n}$, compared to that of a single large turbine. Saving weight leads to a reduction of the production cost. Smulders et al. [6] analyzed a two-rotor configuration in a wind tunnel. In 2010, the South-West Research Institute conducted an analysis of a seven-rotor configuration in the NASA Langley wind tunnel to test the MRS concept and found no negative interferences among the rotors [7]. Numerical simulations of the aerodynamic performance for the same seven-rotor system were presented by Chasapogiannis et al. [8]. In their computational fluid dynamics simulations using actuator disks, a power increase of 3% was predicted for the seven-rotor system. Yoshida et al. [9] investigated coherence effects on the power and tower loads of a MRS. On a larger scale, structural considerations of a 20 MW multirotor system with 45 rotors have been presented by Jamieson and Branney [3]. They showed that mass and cost are reduced, in comparison with a single-rotor turbine with the same power, and that the structure is designed based on the aerodynamic forces rather than on the rotor loading. It can be anticipated that a multirotor system is capable of solving such problems involved in such supersized wind turbines at some level. However, with typical multirotor systems, such an arrangement provides only overall output without any synergistic effects, which is simply represented by the product of the output of each wind turbine and the number of wind turbines. That is to say, with the number of wind turbines in the system as "n," the output of the overall system is a multiple n of the output of each single wind turbine. It should be noted that improvement of such conventional multirotor systems has limitations in power output increase and provide only a small increase in efficiency on the order of at most 1–3% [10–12].

As another wind turbine concept, there is an invention of diffuser-augmented wind turbines (DAWTs), of which rotor is shrouded by a diffuser [13–18]. DAWTs show power increase compared with conventional turbines. We have been developing a brimmed-diffuser augmented wind turbine (B-DAWT) called wind-lens turbine (WLT) [19,20]. In the present research, we develop a new wind turbine system that is a combination of a MRS and WLTs. We placed two [11] or three WLTs closely in some arrangements perpendicular to the flow and measured each power output and drag simultaneously. In parallel with experiments, we are doing computational fluid dynamics of the MRS with WLTs using the actuator-disk method.

2 Experimental Setup

The large boundary-layer wind tunnel of the Research Institute for Applied Mechanics, Kyushu University, was used in this work. The wind tunnel had a test section of 15 m long × 3.6 m wide × 2 m high, with a maximum wind velocity of 30 m/s, and was characterized by a low turbulence intensity of 0.4%. To minimize blockage effects, half of the test section's side walls and ceiling panels were removed. The previous measurement of wind velocity and static pressure had already verified that no noticeable blockage existed.

Figure 1 shows schematics of the dimensions of three WLTs in a side-by-side (SBS) arrangement. Each one of the WLTs consisted of a diffuser with a streamwise length L_t of $0.22D_{\text{throat}}$ and a

Contributed by the Advanced Energy Systems Division of ASME for publication in the Journal of Energy Resources Technology. Manuscript received June 1, 2018; final manuscript received January 6, 2019; published online April 4, 2019. Assoc. Editor: Christopher Niezrecki.

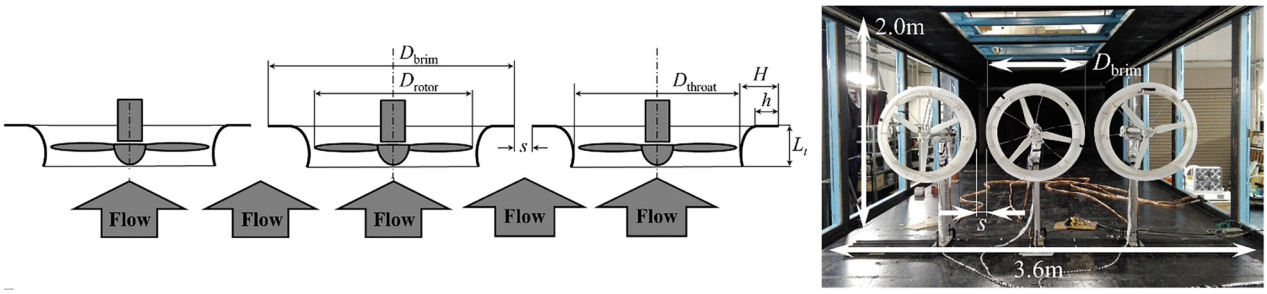

Fig. 1 Schematics of three WLTs in SBS (left) and its photo in the wind tunnel (right)

Table 1 Experimental conditions in a wind tunnel

Conditions	
Configuration of wind acceleration device	CiiB10 type [20]
Inflow velocity	$U_0 = 6$ (m/s)
Reynolds number	1.7×10^5 (representative length: rotor diameter 510 (mm))
Layouts of WLT	3-SBS, 3–90 deg, 3–60 deg
Gap ratio of MRS with WLTs (gap divided by the outer diameter of a brimmed diffuser)	$s/D_{brim} = 0.0 \sim 0.4$

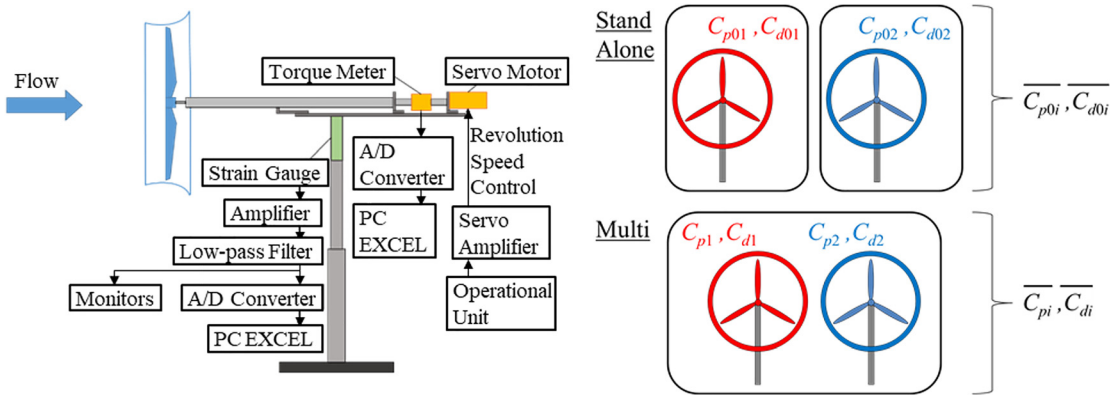

Fig. 2 Procedure of measuring C_p and C_d in each setup (right) and schematic of the measurement system for the power output and the drag force (left)

brim height h of $0.1D_{throat}$, called CiiB10 type WLT [19]. The rotor diameter (D_{rotor}) was 510 mm. The representative diameter of a WLT was $D_{brim} = 696$ mm in the present experiments. Three WLTs were placed in SBS and/or triangle arrangements with gap width s. Table 1 shows the conditions of the presented wind tunnel experiment. The approaching wind speed, U_0, was 6 m/s with a Reynolds number of 1.7×10^5 related to rotor diameter D_{rotor}. The gap ratio was s/D_{brim} (gap width/brim diameter). The range of s/D_{brim} was between 0.01 and 0.3.

The rotor shaft and the motor were linked with a torque meter, as shown in Fig. 2 (left). At constant rotational velocity of the servomotor, the torque was measured for 30 s at 1 kHz sampling frequency. It should be noted that the rotational directions of all the turbines in both stand-alone (SA) and MRS configurations were the same clockwise direction from upstream view. The drag force (thrust force) was measured with a strain gage connected to an amplifier and low-pass filter. All the data were fed into a personal computer through an analog-digital converter. The optimum tip speed ratio λ was determined by setting the appropriate rotational speed of the rotor. For the measurement period, the motor speed was held constant by the servomotor controller. The power coefficient C_p and drag coefficient C_d were calculated using Eqs. (1) and (2). In these equations, P is the power output, T_r is the torque, ω is the angular velocity, F_{drag} is the drag force, ρ is the air density, and A is the swept area of the rotor

$$C_p = \frac{P}{\frac{1}{2}\rho {U_0}^3 A} = \frac{T_r \omega}{\frac{1}{2}\rho {U_0}^3 A} \tag{1}$$

$$C_d = \frac{F_{drag}}{\frac{1}{2}\rho {U_0}^2 A} \tag{2}$$

Figure 2 shows how the power and drag measurements were taken in each setup. For WLTs in stand-alone configurations, the power coefficient was defined C_{p0i} and the drag coefficient was defined C_{d0i} in each turbine. The averages of each coefficient of all turbines were defined $\overline{C_{p0i}}$, $\overline{C_{d0i}}$. For WLTs in multirotor configurations, the power coefficient was defined C_{pi} and the drag coefficient was defined C_{di} in each turbine. The averages of each coefficient of all turbines were defined $\overline{C_{pi}}$, $\overline{C_{di}}$. In order to understand how the power coefficient changed in each turbine, C_{pi} was

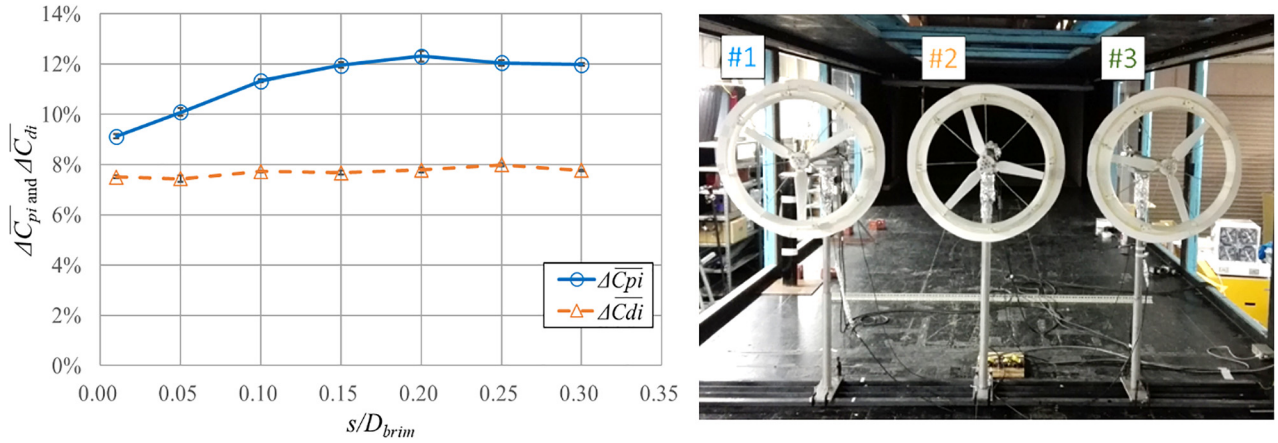

Fig. 3 Experimental setup (right) and relative changes in $\overline{C_{pi}}$ and $\overline{C_{di}}$ for the configuration of three WLTs in SBS arrangement, compared to those for the stand-alone configuration (left)

compared to the C_{p0i}. Therefore, the relative change, ΔC_{pi} was defined as

$$\Delta C_{pi} = \frac{C_{pi}}{C_{p0i}} - 1 \tag{3}$$

To compare the average power coefficient of the MRS with the average power coefficient of the stand-alone WLTs, the relative change, $\Delta\overline{C_{pi}}$ was defined as

$$\Delta\overline{C_{pi}} = \frac{\overline{C_{pi}}}{\overline{C_{p0i}}} - 1 \tag{4}$$

For the drag coefficients, similar to the power coefficients, the relative changes in C_{di} were calculated for ΔC_{di} and $\Delta\overline{C_{di}}$.

3 Results of Wind Tunnel Experiment

3.1 Three Wind-Lens Turbines With CiiB10 in Side-by-Side. Three WLTs with CiiB10 are arranged SBS. As viewed from upstream, WLTs are #1, #2, and #3 from the left side (see Fig. 3). The averages of each coefficient of all turbines were $\overline{C_{p0i}} = 0.48$, and $\overline{C_{d0i}} = 1.8$. Figure 4 shows the results of relative changes in power coefficient, and Fig. 5 shows relative changes in drag coefficient. On the whole, power coefficients and drag coefficients in SBS increased at all gap ratios, and $\Delta\overline{C_{pi}}$ and $\Delta\overline{C_{di}}$ were larger compared with two WLTs case with CiiB10 [11]. Three WLTs seem to accelerate the gap flow, leading to stronger shear flow and vortex shedding. When WLTs are set up closely to each other (e.g., $s/D_{\text{brim}} = 0.01$), relative changes in $\overline{C_{pi}}$ and $\overline{C_{di}}$ were lower. When the $s/D_{\text{brim}} = 0.20$, $\Delta\overline{C_{pi}}$ increased by 12.3% at the maximum and $\Delta\overline{C_{di}}$ increased 7.8%, there seems to be an optimal spacing for $s/D_{\text{brim}} = 0.20$. Additionally, relative changes in $\overline{C_{pi}}$ were always larger compared with those in $\overline{C_{di}}$ at all gap ratios. It was because the power output is proportional to the cube of wind velocity and the drag force is proportional to the square of it. As for individual increases in C_{pi} and $\overline{C_{di}}$, #2 was the highest in almost all cases. This was caused by biased gap flows toward inside. The center WLT #2 in SBS arrangement was influenced most strongly due to wake interference of three WLTs. It is noted that unstable behavior of gap flow between wind turbines has an effect on the performance of wind turbines similar to the studies of Göltenbott et al. [12].

3.2 Triangle Arrangements Using Three Wind-Lens Turbines With CiiB10. Three WLTs with CiiB10 were arranged in two triangle arrangements. One was the right-angle triangle configuration with the open angle of 90 deg, as shown in Fig. 6. The other was the equilateral triangle configuration with the open angle of 60 deg, as shown in Fig. 7. As viewed from the upstream, WLTs are #1, #2, and #3 from the left side. Figures 8 and 9 show the results of relative changes in power coefficient and relative changes in drag coefficient for the two kinds of triangle configurations. At this moment, similar to the results of SBS I

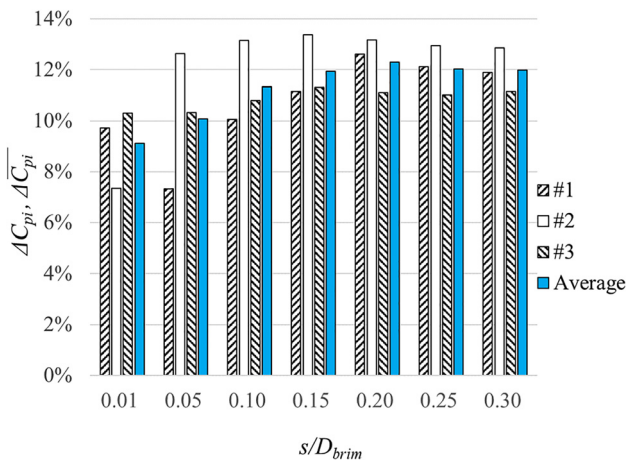

Fig. 4 ΔC_{pi} and $\Delta\overline{C_{pi}}$ for three WLTs with CiiB10

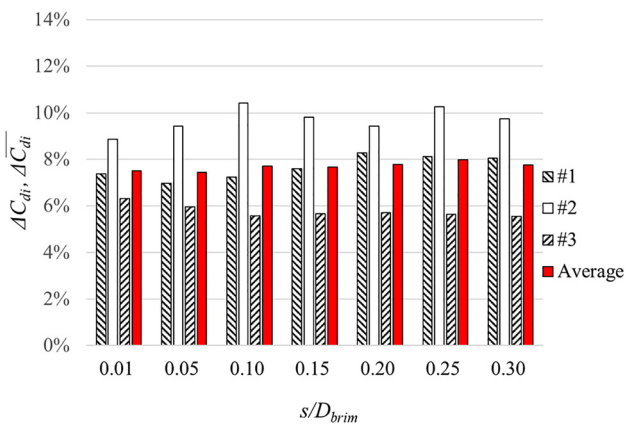

Fig. 5 ΔC_{di} and $\Delta\overline{C_{di}}$ for three WLTs with CiiB10 in SBS

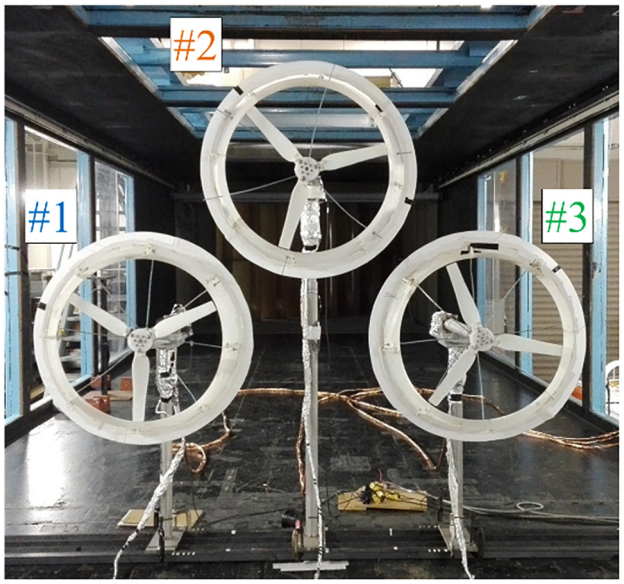

Fig. 6 Experimental setup of M-WLT (3–90 deg)

Fig. 7 Experimental setup of M-WLT (3–60 deg)

aforementioned, power coefficients and drag coefficients in triangle configurations also increased at all gap ratios, as shown in Figs. 8 and 9. When the s/D_{brim} was around 0.2, $\Delta\overline{C_{pi}}$ increased by 10% at the maximum and $\Delta\overline{C_{di}}$ increased by 6% for both triangle configurations. There seemed to be an optimal spacing for $s/D_{\text{brim}} = 0.15 - 0.20$. $\Delta\overline{C_{pi}}$ and $\Delta\overline{C_{di}}$ were a little smaller compared with three WLTs for SBS configuration. The results of individual increases in C_{pi} and C_{di} are shown in Figs. 10–13. Although no obvious drift appeared in ΔC_{di} (Fig. 11), ΔC_{p2} was higher than ΔC_{p1} and ΔC_{p3} over $s/D_{\text{brim}} = 0.1$(Fig. 10) for the right-angle triangle configuration. This meant that the flow around WLT #2 in the right-angle triangle configuration was influenced most strongly from both side of WLTs #1 and #3. On the other hand, when we set the WLTs in an equilateral triangular formation, the WLT which had the highest rate of increase was not

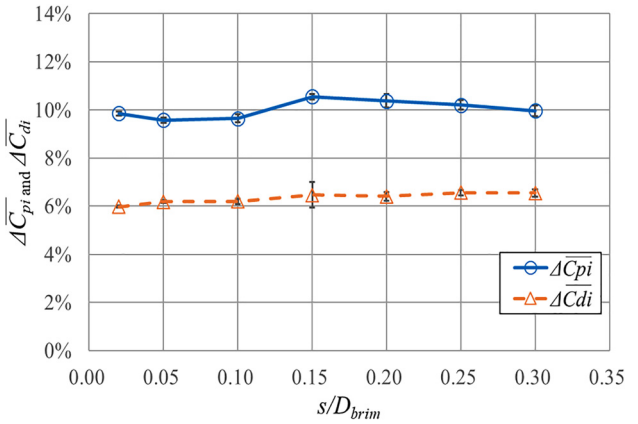

Fig. 8 Relative changes in $\overline{C_{pi}}$ and $\overline{C_{di}}$ compared to those for the stand-alone configuration (3–90 deg)

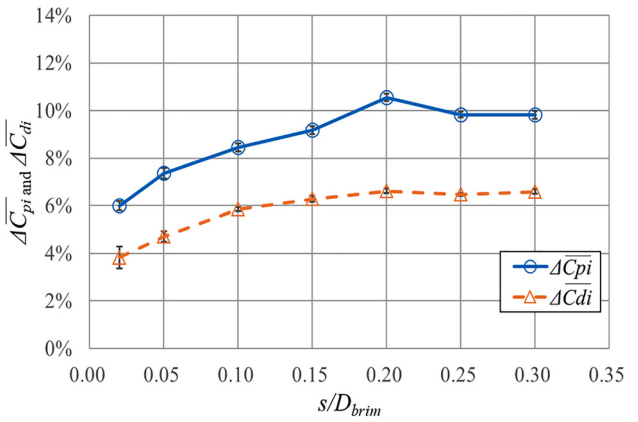

Fig. 9 Relative changes in $\overline{C_{pi}}$ and $\overline{C_{di}}$ compared to those for the stand-alone configuration (3–60 deg)

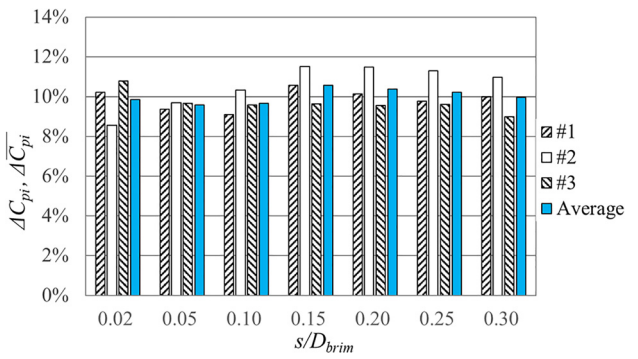

Fig. 10 Individual relative changes in C_{pi} and $\overline{C_{pi}}$ compared to those for the stand-alone configuration (3–90 deg)

always the same one (Figs. 12 and 13). The configuration itself was considered to be the reason of this result; all the WLTs had two WLTs next to themselves in this balanced position, possibly being affected by two gap flows.

4 Numerical Analyses

Flows around a MRS with three WLTs in SBS arrangements were numerically simulated using a three-dimensional large eddy simulation (LES) based on the finite difference method (FDM).

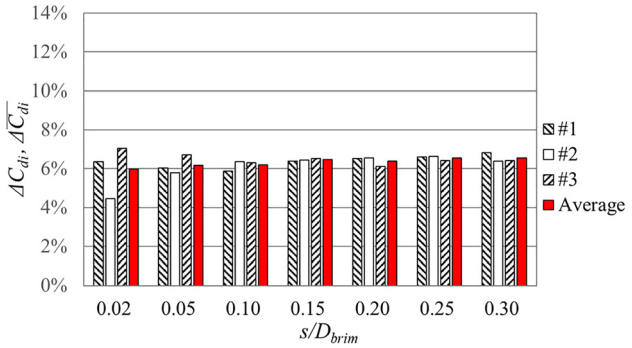

Fig. 11 Individual relative changes in C_{di} and $\overline{C_{di}}$ compared to those for the stand-alone configuration (3–90 deg)

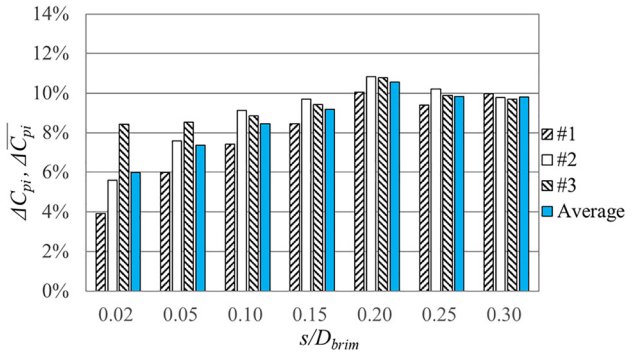

Fig. 12 Individual relative changes in C_{pi} and $\overline{C_{pi}}$ compared to those for the stand-alone configuration (3–60 deg)

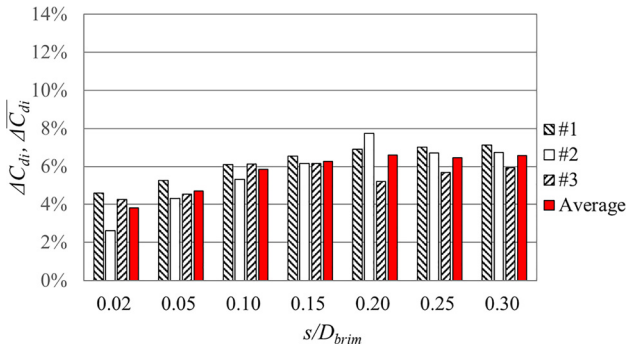

Fig. 13 Individual relative changes in C_{di} and $\overline{C_{di}}$ compared to those for the stand-alone configuration (3–60 deg)

Table 2 shows the numerical conditions. We used FORTRAN code which we had developed. The governing equations were the continuity and Navier–Stokes equations. A first-order explicit method was used for time marching. A third-order upwind scheme was applied to the convective term. The wind turbine was modeled on the actuator disk method [21]. The shroud bodies were modeled on the rectangular grid approximation. To avoid any blockage effects, a large computational domain was adopted, as described below in Fig. 14. A grid refinement study was done to be confirmed that no noticeable difference appeared in the numerical result on twice higher accuracy grid. Consequently, the overall tendency and qualitative results showed good agreements with those from the wind tunnel experiments.

Figure 15 shows an instantaneous flow around the MRS with three WLTs at $s/D_{\text{brim}} = 0.05$. The flow field was visualized at the

Table 2 Numerical conditions

Conditions	
Discretization technique	Finite difference method
Time marching method	Euler explicit scheme
Coupling method	Fractional step method
Coordination system	Three-dimensional Cartesian coordinate system
Variable arrangement	Staggered
Turbulence model	LES
SGS model	Mixed-time-scale SGS model
Convection term	Third order upwind differencing scheme
Reynolds number	3.0×10^5 (representative length: rotor diameter)
Grid resolution	$\Delta x = \Delta y = \Delta z = 0.01 D_{\text{brim}}$ (near turbine)
Number of grid points	$226 \times 571 \times 211$
Computational domain	$10D_{\text{rotor}} \times 25D_{\text{rotor}} \times 10D_{\text{rotor}}$
Boundary conditions	Inflow velocity: uniform wind condition
	Outflow velocity: Sommerfeld radiation condition
	Velocity at side wall: flee-slip condition
	Velocity at body surface: no-slip condition
	Pressure: Neumann condition

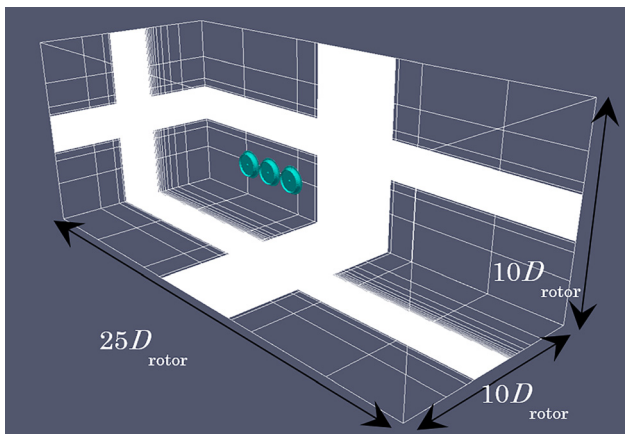

Fig. 14 Computational domain for three WLTs in SBS arrangement

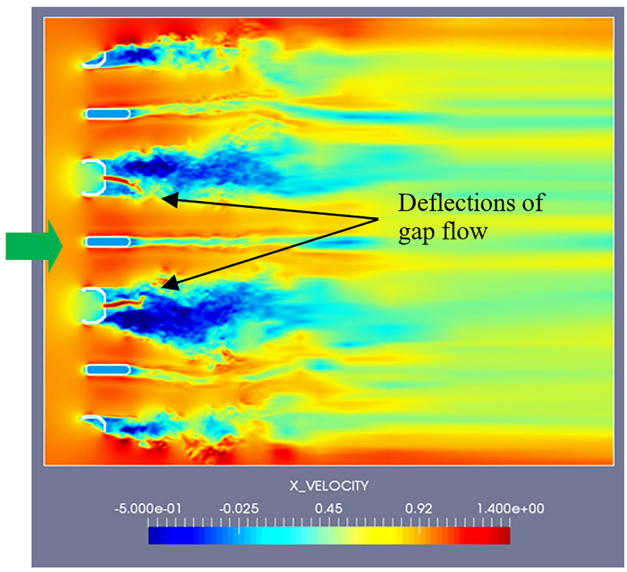

Fig. 15 Instantaneous streamwise wind velocity ($s/D_{\text{brim}} = 0.05$), flow is left to right

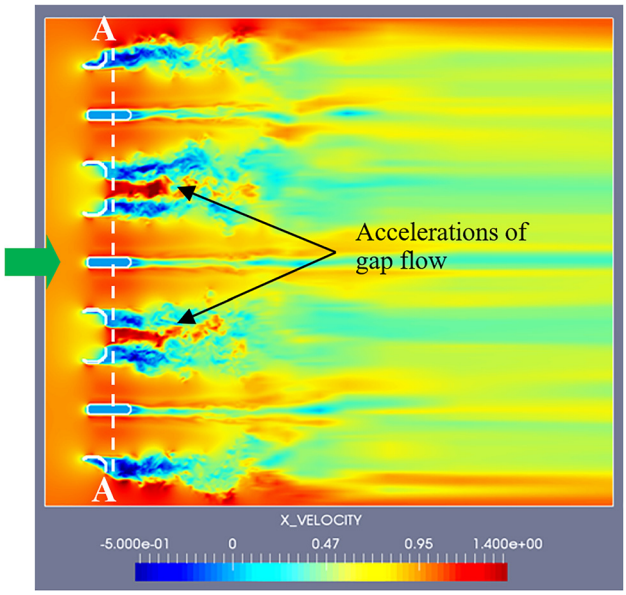

Fig. 16 Instantaneous streamwise wind velocity ($s/D_{brim} = 0.2$), flow is left to right

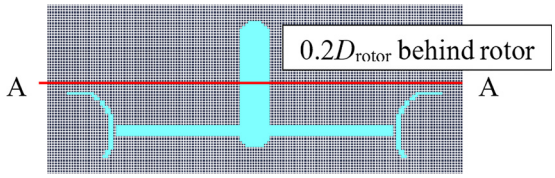

Fig. 18 Grid resolution around a single WLT of CiiB10 (The pressure distributions in Fig. 17 were evaluated along the line A–A behind the single WLT with $0.2D_{rotor}$ separation)

Fig. 19 Nine kilowatt multilens turbine using three 3 kW WLTs at Kita-kyushu city, March 2017

center height of three turbines in SBS arrangement. The two gap flows were biased inside in SBS arrangement. It meant that the center WLT showed higher C_{pi} and C_{di} compared to those for both side WLTs, as shown in Figs. 4 and 5. Generally, in the wake interference, the body with the biased side of gap flow shows higher drag as reported by Ohya et al. [11,22–24]. The results as shown in Figs. 4, 5, and 15 show good consistency.

Figure 16 shows an instantaneous flow around the MRS with three WLTs at $s/D_{brim} = 0.2$. The flow field was visualized at the center height of three turbines in SBS arrangement. The two gap flows were strongly accelerated due to the flow interaction with a pair of WLTs. To investigate the pressure distribution behind the MRS with three WLTs, we evaluated a nondimensional static pressure along the line A–A, which was just behind the turbines, as described in Fig. 16. Figure 17 shows the time-averaged pressure distribution. Here, the black line of MRS-3-180 shows the pressure distribution of a MRS with three WLTs. Other three dotted lines of SA (stand-alone configuration) mean the pressure distributions of a single WLT in the stand-alone configuration, as explained in Fig. 18. To compare those values and profiles of the static pressures, the SA pressure distributions were aligned with the same positions with three WLTs in the SBS arrangement. From Fig. 17, it is clearly seen that the pressure behind the MRS with three WLTs was remarkably lowered compared to those for SA configurations. Thus, the gap flows were accelerated, leading

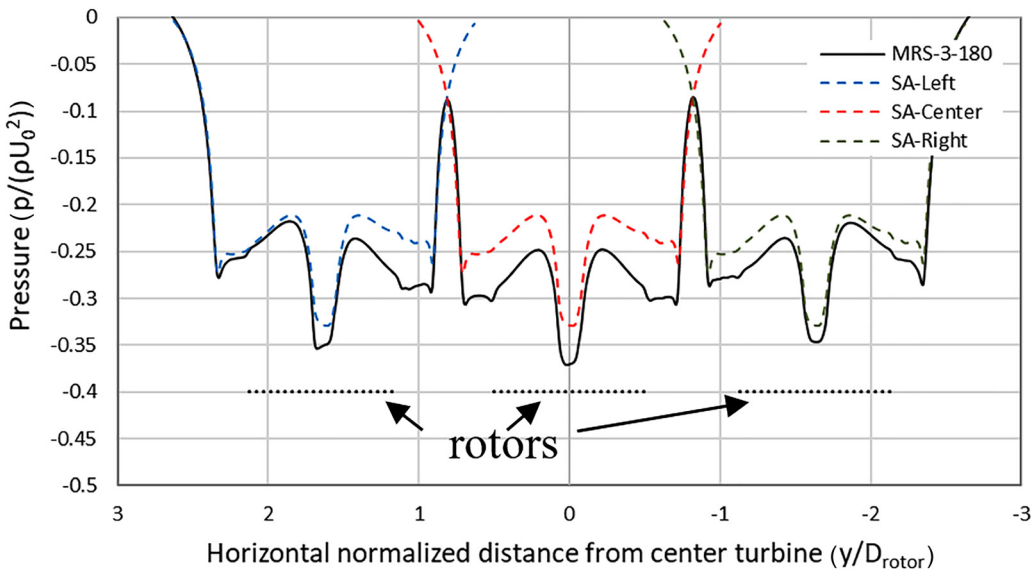

Fig. 17 Cross-streamwise profiles of normalized pressure behind the MRS with three WLTs in SBS arrangements with gap ratio of $s/D_{brim} = 0.2$

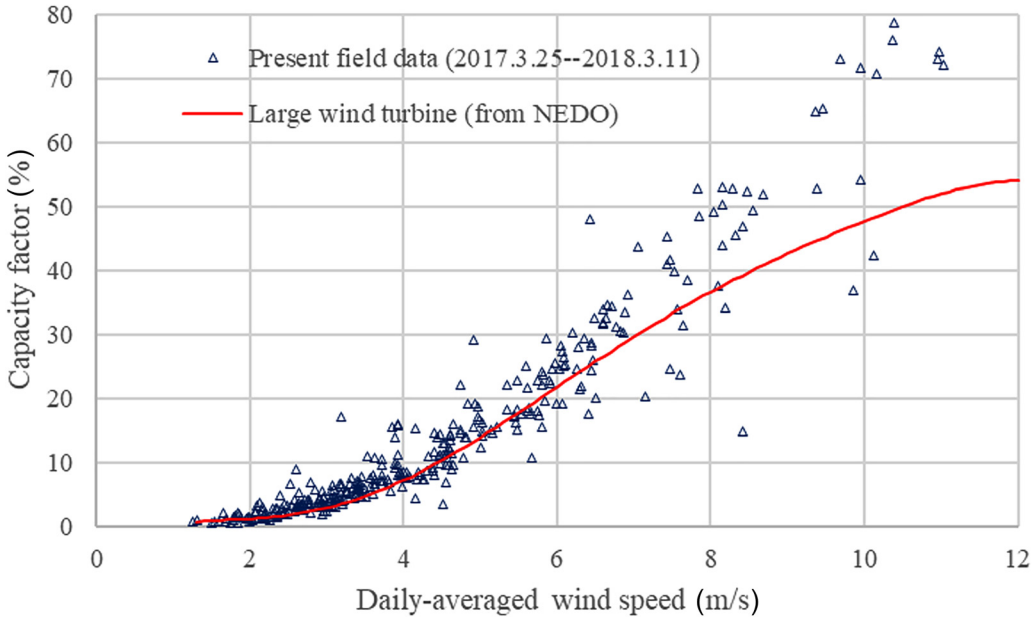

Fig. 20 The capacity factor of a 9 kW multilens turbine using three 3 kW WLTs at Kita-kyushu city, March 2017 to March 2018. The rated wind speed is 11.0 m/s.

to vortices near the gaps, causing the lower pressure regions behind the WLTs. It meant that the lowered pressured regions drew much more airflows into turbines in the MRS with WLTs. Therefore, the C_{pi} and C_{di} for a MRS with WLTs showed higher values compared to those for the stand-alone configuration.

5 Field Test

Very recently, we have manufactured a prototype of a 9 kW MRS system using three 3 kW WLTs and have installed in the field in Kita-Kyushu city, Japan, as shown in Fig. 19. The diameter of each WLT was 2.78 m, and the top height of MRS was 18 m. As shown in Fig. 20, the results of power output have already shown higher capacity factors over a wide range of wind speed, compared to that for bigger wind turbines of MW class. The description of field experiments here is a partial consequence. Circumstantial methods and results will be described in our next paper.

6 Conclusion

Multirotor systems for wind turbine configurations have been studied for SBS and two triangle arrangements (90-deg and 60-deg) of DAWTs which are called WLTs. First, the power coefficient and drag coefficient (thrust force) for the three MRS with WLTs in SBS arrangements were investigated, followed by the similar study for two triangle configurations using three WLTs. A large boundary layer wind tunnel in Kyushu University was used for all the experiments. In parallel with wind tunnel experiments, we conducted LES of MRS with WLTs using the actuator-disk method, based on FDM.

Closely spaced DAWT with brim (WLTs), i.e., the MRS with three WLTs in SBS configuration showed a remarkable increase in power output with the gap ratio s/D_{brim}. The largest average increase was achieved at a range of $s/D_{\text{brim}} = 0.15 - 0.3$, reaching up to 12%. The average drag was also increased 8% for the three-WLT configuration. It should be noted that the individual increases in C_p and C_d showed distinct differences with each other. The higher values in C_p corresponded to higher values in C_d for both configurations in SBS. The increase in C_p was much larger than those in C_d because the power out is proportional to the cube of the incoming wind velocity into the wind turbine and the drag is proportional to the square of it. The relative changes in C_p and C_d with the three-WLT configuration became larger compared to those with the two-WLT configuration in SBS arrangement.

Two MRSs of triangle arrangements using three WLTs with CiiB10 were investigated similarly to the SBS arrangement. One was the right-angle triangle configuration with the open angle of 90 deg. The other was the equilateral triangle configuration with the open angle of 60 deg. Power coefficients and drag coefficients in triangle configurations also increased at all gap ratios. When the s/D_{brim} was around 0.2, ΔC_p was increased by 10% at the maximum and ΔC_d was increased by 6% for both triangle configurations. ΔC_p and ΔC_d were a little smaller compared with three WLTs for SBS configuration.

The increase in the power coefficient and the drag coefficient for the three-WLT MRS configurations in close proximity can be explained by the flow interference around bluff bodies and gap flow behaviors. Similarities can be drawn between the flow around three-dimensional bluff bodies (for example, circular plates) in SBS and the flow around multiple WLTs in SBS. The gap flows between WLTs with close vicinity play an important role to cause the increases in the power coefficient and the drag coefficient.

To investigate the wake interference for MRS with WLTs, numerical analyses of the flow around a MRS with three WLTs in SBS arrangement were made using LES based on FDM. At $s/D_{\text{brim}} = 0.05$, the two gap flows were clearly biased toward the center WLT, leading to higher C_p and C_d of the center WLT. At $s/D_{\text{brim}} = 0.2$, the two gap flows were strongly accelerated due to the flow interaction with a pair of WLTs. To investigate the pressure distribution behind the MRS with three WLTs, we evaluated the nondimensional pressure just behind the WLTs in SBS. The pressure was remarkably lowered compared to those for stand-alone configurations. The accelerated gap flows caused the lower pressure regions behind the WLTs. The lower pressured regions drew much more airflows into turbines in the MRS with WLTs. Therefore, the C_p and C_d for a MRS with WLTs showed higher values compared to those for the stand-alone configuration.

Our recent prototype is nearly to be another evidence to show how the MRS can be a good answer to supersede of one big typical turbine.

The total number of wind turbines used in the present research is three. One question arises: how will a MRS behave with more than three turbines? The focus of our future research will be addressing these issues.

Acknowledgment

We gratefully acknowledge our laboratory staff Messrs. K. Matsushima and K. Watanabe along with the students Dr. U. Göltenbott, Mr. A. Munakata, and Mr. J. Miyazaki for their cooperation and assistance in the experiments and in the analysis of the data. This research is in cooperation with Dr. Peter Jamieson who belongs to the University of Strathclyde, UK.

Funding Data

- New Energy and Industrial Technology Development Organization (NEDO) (Funder ID: 10.13039/501100001863).

Nomenclature

A = swept area of rotor (m^2)
C_d = drag coefficient
C_{di} = drag coefficient of each turbine in the multibody configuration
C_{d0i} = drag coefficient of a turbine in the stand-alone configuration
C_p = power coefficient
C_{pi} = maximum power coefficient of each turbine in the multirotor configuration
C_{p0i} = maximum power coefficient of a turbine in the stand-alone configuration
$\overline{C_{di}}$ = average drag coefficient of multiple turbines in the multibody configuration
$\overline{C_{d0i}}$ = average drag coefficient of all turbines in the stand-alone configuration
$\overline{C_{pi}}$ = average of maximum power coefficients of all turbines in the multirotor configuration
$\overline{C_{p0i}}$ = average of maximum power coefficients of all turbines in the stand-alone configuration
D_{brim} = brim diameter for WLT (m)
D_{rotor} = rotor diameter (m)
D_{throat} = diffuser throat diameter (m)
f = frequency (Hz)
F_{drag} = drag force (N)
h = brim height (m)
L = reference length (m)
L_t = length of diffuser (m)
P = power output (W)
r = radius of the rotor (m)
Re = Reynolds number = $U_0 L/\nu$
s = gap width (m)
s/D_{brim} = gap ratio for wind-lens turbines in the multirotor configuration
T_r = torque (N·m)
U = wind velocity in streamwise direction (x-direction) (m/s)
U_0 = approaching wind velocity (x-direction) (m/s)
x, y, z = streamwise, spanwise, and vertical directions (m)
ΔC_{di} = relative change in C_{di} compared to C_{d0i} (%)
ΔC_{pi} = relative change in C_{pi} compared to C_{p0i} (%)
$\Delta\overline{C_{di}}$ = relative change in $\overline{C_{di}}$ compared to $\overline{C_{d0i}}$ (%)
$\Delta\overline{C_{pi}}$ = relative change in $\overline{C_{pi}}$ compared to $\overline{C_{p0i}}$ (%)
λ = tip speed ratio
ν = kinematic viscosity (m^2/s)
ρ = air density (kg/m^3)
ω = angular velocity $2\pi f$ (rad/s)

References

[1] Hofmann, M., and Sperstad, I. B., 2014, "Will 10 MW Wind Turbines Bring Down the Operation and Maintenance Cost of Offshore Wind Farms?," Energy Procedia, **53**, pp. 231–238.
[2] Sieros, G., Chaviaropoulos, P., Sørensen, J. D., Bulder, B. H., and Jamieson, P., 2012, "Upscaling Wind Turbines: Theoretical and Practical Aspects and Their Impact on the Cost of Energy," Wind Energy, **15**(1), pp. 3–17.
[3] Jamieson, P., and Branney, M., 2012, "Multi-Rotors; A Solution to 20 MW and Beyond?," Energy Procedia, **24**, pp. 52–59.
[4] Heronemus, W., 1972, "Pollution-Free Energy From Offshore Winds," Eighth Annual Conference and Exposition, Marine Technology Society, Washington, DC, Dec. 26–31.
[5] Jamieson, P., 2018, *Innovation in Wind Turbine Design*, 2nd ed., Wiley, Chichester, UK, pp. 297–312.
[6] Smulders, P. T., Orbons, S., and Moes, C., 1984, "Aerodynamic Interaction of Two Rotors Set Next to Each Other in One Plane," European Wind Energy Conference, Hamburg, Germany, Oct. 22–26, pp. 529–533.
[7] Ransom, D., Moore, J. J., and Heronemus-Pate, M., 2010, "Performance of Wind Turbines in a Closely Spaced Array," Renewable Energy World, **2**(3), pp. 32–36.
[8] Chasapogiannis, P., Prospathopoulos, J. M., Voutsinas, S. G., and Chaviaropoulos, T. K., 2014, "Analysis of the Aerodynamic Performance of the Multi-Rotor Concept," J. Phys.: Conf. Ser., **524**, p. 012084.
[9] Yoshida, S., Goltenbott, U., Ohya, Y., and Jamieson, P., 2016, "Coherence Effects on the Power and Tower Loads of a 7 × 2 MW Multi-Rotor Wind Turbine System," Energies, **9**(9), p. 742.
[10] Munakata, A., Miyazaki, J., Göltenbott, U., Ohya, Y., and Uchida, T., 2016, "MRS Using DAWTs for Power Increase," 15th World Wind Energy Conference and Exhibition (WWEC2016), Tokyo, Japan, Oct. 31–Nov. 1.
[11] Ohya, Y., Miyazaki, J., Göltenbott, U., and Watanabe, K., 2017, "Power Augmentation of Shrouded Wind Turbines in a Multirotor System," ASME J. Energy Resour. Technol., **139**(5), p. 051202.
[12] Göltenbott, U., Ohya, Y., Yoshida, S., and Jamieson, P., 2017, "Aerodynamic Interaction of Diffuser Augmented Wind Turbines in Multi-Rotor Systems," Renewable Energy, **112**, pp. 25–34.
[13] Gilbert, B. L., and Foreman, K. M., 1983, "Experiments With a Diffuser-Augmented Model Wind Turbine," ASME J. Energy Resour. Technol., **105**(1), pp. 46–53.
[14] Hansen, M. O. L., Sørensen, N. N., and Flay, R. G. J., 2000, "Effect of Placing a Diffuser Around a Wind Turbine," Wind Energy, **3**(4), pp. 207–213.
[15] Abe, K., Nishida, M., Sakurai, A., Ohya, Y., Kihara, H., Wada, E., and Sato, K., 2005, "Experimental and Numerical Investigations of Flow Fields Behind a Small Wind Turbine With a Flanged Diffuser," J. Wind Eng. Ind. Aerodyn., **93**(12), pp. 951–970.
[16] van Bussel, G. J. W., 2007, "The Science of Making More Torque From Wind: Diffuser Experiments and Theory Revisited," J. Phys.: Conf. Ser., **75**, p. 012010.
[17] Sedaghat, A., Waked, R. A. I., Assad, M. E. I. H., Khanafer, K., and Salim, M. N. A. B., 2017, "Analysis of Accelerating Devices for Enclosure Wind Turbines," Int. J. Astronaut. Aeronaut. Eng., **2**(2), p. 9.
[18] Khamlaj, A. T., and Rumpfkeil, P. M., 2018, "Analysis and Optimization Study of Shrouded Horizontal Axis Wind Turbines," AIAA Paper No. 2018-0996.
[19] Ohya, Y., Karasudani, T., Sakurai, A., Abe, K., and Inoue, M., 2008, "Development of a Shrouded Wind Turbine With a Flanged Diffuser," J. Wind Eng. Ind. Aerodyn., **96**(5), pp. 524–539.
[20] Ohya, Y., and Karasudani, T., 2010, "A Shrouded Wind Turbine Generating High Output Power With Wind Lens Technology," Energies, **3**(4), pp. 634–649.
[21] Ohya, Y., Uchida, T., Karasudani, T., Hasegawa, M., and Kume, H., 2012, "Numerical Studies of Flow Around a Wind Turbine Equipped With a Flanged-Diffuser Shroud Using an Actuator-Disk Model," Wind Eng., **36**(4), pp. 455–472.
[22] Hayashi, M., Sakurai, A., and Ohya, Y., 1986, "Wake Interference of a Row of Normal Flat Plates Arranged Side by Side in a Uniform Flow," J. Fluid Mech., **164**(1), pp. 1–25.
[23] Ohya, Y., Okajima, A., and Hayashi, M., 1989, "Wake Interference and Vortex Shedding," *Encyclopedia of Fluid Mechanics*, Vol. 8, N. P. Cheremisinoff, ed., Gulf Publishing Corporation, Houston, TX, pp. 323–389.
[24] Ohya, Y., 2014, "Bluff Body Flow and Vortex—Its Application to Wind Turbines," Fluid Dyn. Res., **46**(6), p. 061423.